An Acad Bras Cienc (2020) 92(3): e20200524 DOI 10.1590/0001-3765202020200524
Anais da Academia Brasileira de Ciências | *Annals of the Brazilian Academy of Sciences*
Printed ISSN 0001-3765 I Online ISSN 1678-2690
www.scielo.br/aabc | www.fb.com/aabcjournal

ENGINEERING SCIENCES

Two steps CrAlFeSi coating on low carbon steel prepared by mechanical alloying and its oxidation properties

DIDIK ARYANTO, ALFIAN NOVIYANTO, RISMA Y. SUNDAWA, TOTO SUDIRO, AGUS S. WISMOGROHO, WAHYU B. WIDAYATNO & PERDAMEAN SEBAYANG

Abstract: Two steps CrAlFeSi coating has been fabricated on low carbon steel via mechanical alloying methods and its oxidation properties have been elucidated thoroughly. First, Al coating was deposited on the low carbon steel substrate via mechanical alloying for 1 h. Afterward, CrAlFeSi coating was deposited on Al coating using the same technique for 2 h. The effect of annealing at 650 °C on the oxidation behavior of two steps CrAlFeSi coatings was examined thoroughly. The microstructure of the coating layer before and after annealing was relatively similar. Microholes and microcracks were found in the coating layer of the substrate before and after annealing. Intermetallic phases were observed in the samples along with the major elements. The mass gain after cyclic oxidation at 800 °C in the air atmosphere for a substrate with two coating layers reduced by a factor of 10 compared to the substrate without coating layer, which is likely due to the formation of Al_2O_3 on the outer layer during the oxidation process. The thin layer of Al_2O_3 protects the inner layer from severe oxidation. Therefore, the two steps coating of CrAlFeSi on the low carbon steel can be used as an alternative method for reducing the oxidation at high temperature.

Key words: mechanical alloying, two-steps coating, annealing, oxidation.

INTRODUCTION

Low-carbon steel has been widely used in various applications owing to its excellent mechanical properties and lower cost. However, the utilization of low-carbon steel at high-temperature applications is still very limited due to its poor wear, corrosion and oxidation resistance (Mohammadnezhad et al. 2012). Hence, various surface modification techniques (coatings) such as electro-deposition (Laszczyńska et al. 2016), thermal spraying (Szymański et al. 2015), and cold spraying (Yang et al. 2011), have been undertaken to improve its corrosion and oxidation resistance.

Recently, mechanical alloying (MA) have been applied to deposit metal or intermetallic compound on a substrate (Aryanto & Sudiro 2018, Bafandeh et al. 2017, Canakci et al. 2013, Chen et al. 2016, Li et al. 2012, 2014, Mohammadnezhad et al. 2012, 2013, Romankov et al. 2006, 2009a, b, Saba et al. 2016, Sudiro et al. 2018, Wismogroho et al. 2009, Zadorozhnyy et al. 2017, Zhan et al. 2006). Moreover, MA was successfully utilized to deposit a composite coating layer on the substrate (Chen et al. 2016). The formation of a coating layer using MA depends on the cold-welding process of the particle. The cold-welding process only occurred with the presence of ductile materials. Moreover, ductile material also acts as a binding agent. Al and Cu are binding agents that have been used in coating prepared by MA (Aryanto & Sudiro 2018,

Bafandeh et al. 2017, Chen et al. 2016, Li et al. 2012, Mohammadnezhad et al. 2012, 2013, Romankov et al. 2006, Sudiro et al. 2018, Zadorozhnyy et al. 2017). In general, binding agents are usually mixed directly with supporting materials to strengthen the system, which formed a solid-solution (Mohammadnezhad et al. 2013, Saba et al. 2016) or composite (Chen et al. 2016).

To the best of author knowledge, there are no reports of the two steps coating using MA. The first step is the deposition of a binding agent on the low carbon steel substrate and followed by the deposit of supporting material in the second step coating. The materials used in this study were Cr, Al, Fe, and Si. They were chosen because of the formation of a protective layer during high temperature application. Moreover, Fe was used to reduce the lattice mismatch between the coating and substrate. This study aims to examine the microstructure feature as well as the oxidation properties of the two steps coating on the low carbon steel by means of mechanical alloying technique.

MATERIALS AND METHODS

Preparation of two steps CrAlFeSi Coating

High purity powder (> 99%) of Al, Cr, Fe and Si were used in this experiment. The procedure to prepare and to clean low carbon steel (ST41) substrate (10 × 8 × 3 mm^3) follow our previous reports (Aryanto & Sudiro 2018, Sudiro et al. 2018). The coating on the low carbon steel substrate was done in two steps.

The first step was the deposition of Al as a binding agent on a low-carbon steel substrate using MA for 1 h in a 125 mL cylindrical steel vial (SS 304). In this works, Al-granule (Merck, purity > 99.0%) was used as starting materials. The photograph and SEM image of the Al-powder is shown in Figure 1. A similar Al element was used in first and seconds steps. The second step was the coating of CrAlFeSi on the substrate that already contains the Al coating layer. Prior to this step, Cr, Al, Fe and Si powder were mixed for 1 h using ball milling. The detail composition of Cr, Al, Fe, Si powder is shown in Table I. The coating of Cr, Al, Fe, and Si on the substrate was carried out using MA for 2 h. The MA for the first and second step was performed in an air atmosphere using a high-speed shaker mill with an oscillation frequency of 700/min. The ball to powder ratio was 10 for both the first and second steps. In order to prevent excessive contamination, the steel balls were used with the size of 5 mm in diameter. The coated substrate was annealed at 650 °C for 2 h in the vacuum condition with a heating rate of 5 °C/min and natural furnace

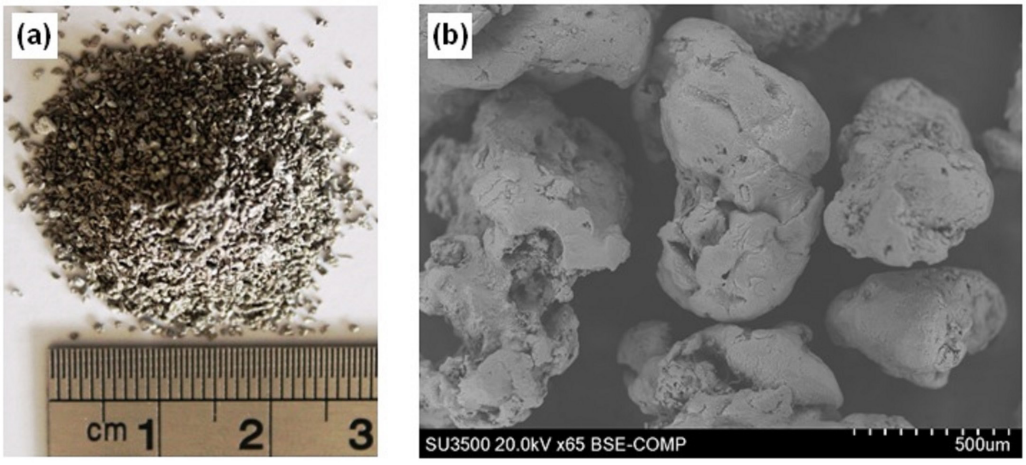

Figure 1. (a) Photograph and (b) SEM image of Al-powder.

Table I. Chemical composition of the milled powder for the second step coating.

Element	Cr	Al	Fe	Si
at.%	35	35	10	20

cooling. The annealed temperature was selected close to the aluminum melting point, i.e., 660 °C (Aryanto & Sudiro 2018). The microstructure and phase evolution of the coated substrate after annealing were examined and compared with the coated substrate without annealing.

Cyclic Oxidation

Cyclic oxidation experiments were carried out in a muffle furnace with an atmospheric environment at 800 °C. Three samples were prepared for each condition in this experiment. Before oxidation, the dimensions of each sample were measured carefully using a digital caliper and then each sample was placed in a square alumina boat crucible separately to prevent contamination. In each cyclic oxidation, the sample was inserted into the furnace for 20 h and then removed for cooling down. After air cooling to the room temperature, the weight gain of the samples was measured three times using an electronic balance with a precision of 0.01 mg and the results were analyzed. This process is repeated up to 8 cycles and a total oxidation time is 160 h.

Characterizations

The cross-sectional microstructure of the coating layer on the substrates was observed using scanning electron microscopy (SEM; SU 3500; Hitachi; Japan) equipped with energy disperse X-ray analysis (EDX; X-maxN; Horiba; Japan). The phase evolution of coated substrates was identified by room-temperature X-ray diffraction (XRD; Smartlab; Rigaku; Japan) with CuKα radiation (λ= 1.5418 Å).

RESULTS AND DISCUSSION

First step coating

Figure 2 displays the SEM image of the substrate after the first step coating using MA. It is clearly seen that the substrate is coated with Al. The Al layer was formed due to collision among balls, substrate and powder. Even though the thickness of the coating layer is not uniform (less than 3 μm), the substrate is well-coated by Al powder. No cracks were observed between the coating-substrate interfaces, as shown in the high magnification SEM image in Figure 2. It is indicated a strong bonding between them. This result confirms the previous research report (Aryanto & Sudiro 2018, Bafandeh et al. 2017, Chen et al. 2016, Li et al. 2012, Mohammadnezhad et al. 2012, 2013, Romankov et al. 2006, Sudiro et al. 2018, Zadorozhnyy et al. 2017), where coating prepared by mechanical alloying provides high bonding ability between coating material and substrate. The basic principle of coating using MA is based on balls-materials-substrate collision, which promotes mechanical bonding between coating materials and substrates (Aryanto & Sudiro 2018). The ductile property of Al-powder makes it flat, overlaps and forms cold welds as the effect of collisions and grinding balls during the MA process (Canakci et al. 2013). As the process continues, the sufficient impacting force causes the trapping Al stick on the substrate, resulting in Al-coating layer. EDX analysis confirmed that the major element in the coating layer is Al, as shown in Figure 2 and Table II. However, a small trace of Fe was found in the coating layer, the contamination of Fe is likely to come from the grinding media (vial and

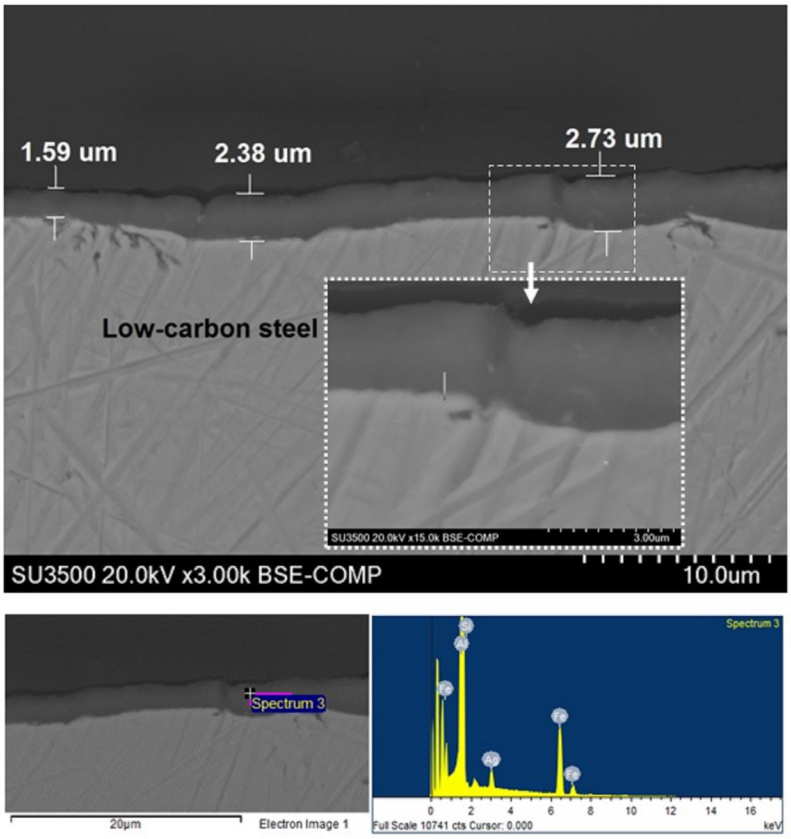

Figure 2. SEM images and EDX point area of Al coating on low-carbon steel.

balls) and substrate, which is inevitable during MA. The high magnification SEM supported the result in Figure 2 and EDX mapping analysis in Figure 3. Small grain with the light gray color in the Al coating layer is Fe-impurity from the ball, vial and substrate material. Their small parts are believed to peel off from the outer surface when exposed to repeated friction and collision in the coating process. They become one with the Al-coating material and are deposited in the coating layer.

Figure 4 shows the XRD patterns of the original substrate and the substrate after the first step coating. In addition to Fe peaks from the substrate, Al peaks were observed in the substrate after the first step coating (Figure 4b). This result shows that Al was deposited on the surface of the substrate after the first step coating, which is also confirmed by the SEM image in Figure 2. No secondary phase, such as intermetallic is observed in Figure 4b, indicating that there is no reaction between Al and the substrate. It can be seen in the high magnification SEM image (Figure 2) and EDX elemental mapping (Figure 3), which shows no diffusion zone was observed in the coating-substrate interface. Thermal energy, as the effect of collisions during the MA process, may not enough giving energy for Al and Fe atoms to react, so they only have mechanical bonding on the interface. Figure 3 also shows that the Al-element was distributed continuously and uniformly on the substrate surface.

Second step coating

Figures 5a and 5b show the cross-section microstructures of the coated substrate before and after annealing, respectively. It should be noted that the Al layer from the first step was disappeared after the second step coating using

Table II. EDX analysis of the first coating layer.

Element	Weight%	Atomic%
Al K	86.70	93.41
Si K	0.38	0.39
Fe K	10.82	5.63
Ag L	2.09	0.56
Totals	100.00	

MA. This fact can be explained due to the severe collision of balls, substrate and powder, which led to the decay of the Al coating layer. Moreover, there is a possibility of CrAlFeSi powder insertion into the Al coating layer and mixing during MA. Since the coating layer contained another element, such as Cr, Fe and Si, the previous Al coating layer from the first step was not found in the second step. The average coating thickness from the second step was 75 µm. Microholes were observed in the coating layer of the coated substrate before annealing (Figure 5a) along with the microcrack in the outer surface and coating/substrate interface. The formation of microholes in the coating can be explained as follows: the hardness of the particles increased due to the work hardening of the particle during milling. The flaking of coating and the deposition of the hardened particles during MA would result in the formation of microholes (Chen et al. 2016). On the other hand, the formation of a crack in the coating layer occurred due to strain and/or hardening of the coating layer. The strain increased with increasing milling time, resulting in the formation of the crack in the outer layer of the coating surface (Li et al. 2014). Simultaneously, the ball milling process also increases the hardening of the coating layer and the tendency of cracking (Bafandeh et al. 2017, Chen et al. 2016, Li et al. 2012, Romankov et al. 2009b). Moreover, the microcrack in the coating layer could also be due to the formation of intermetallic phases during MA. The formation of microholes and microcracks in the coating layer was also observed in the coated substrate after annealing, as shown in Figure 5b. However, the number of microholes and microcrack were reduced compared to the coated substrate before annealing. Overall, the microstructure of the coating layer is improved after annealing at 650 °C. Therefore, Figures 5a and 5b were analyzed using image processing software to calculate the area of pores. The pore area of Figure 5a was 1220 ± 110 μm^2 compared to Figure 5b that has a pore area 504 ± 141 μm^2. Our results indicate that the substrate after annealing has a better microstructure in terms of pore and crack.

The elements distribution in the coated substrate before and after annealing is shown in Figure 6a and Figure 6b, respectively. The elements are evenly distributed in the coating. However, high concentration of Si found in the sample after annealing Figure 6b. The result was supported by SEM image and elemental mapping of the CrAlFeSi powder after the coating process (Figure 7), where a small spot with high brightness seen for Cr, Al, Fe, and Si mapping. Detailed observations in Figure 6 and Figure 7 show that several small spots with the high brightness of the Fe and Si elements have a position in the same place. High brightness of the color was indicated the high concentration in the region. Another possibility, the small spots maybe contains compounds between coating elements, where their reacts during the coating process and followed by thermal annealing for coated substrate before and after annealing, respectively.

Table III shows the elemental analysis of the coating layer before (Figure 5a) and after annealing (Figure 5b). It is evident that the amount of Fe is a function of thickness, wherein the amount of Fe was higher near the coating

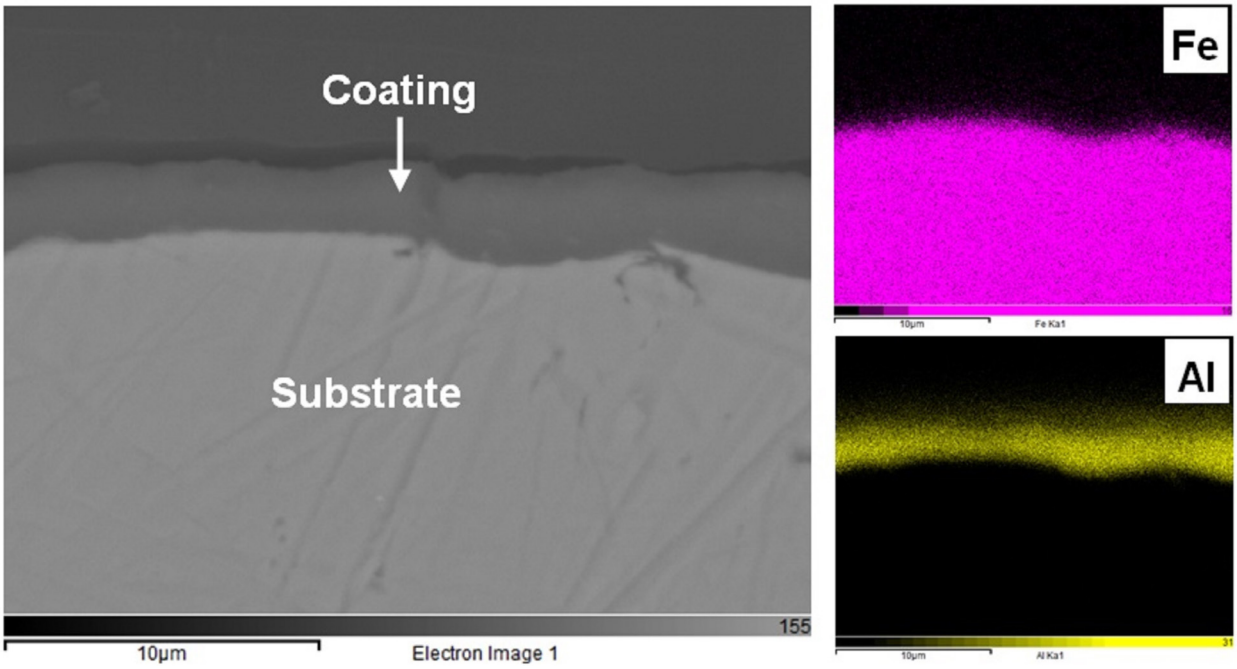

Figure 3. EDX elemental mapping of Al coating on low-carbon steel.

surface compared to the interface of coating and substrate for both before and after annealing. Similar results were obtained for the amount of Al in the annealed substrate. On the contrary, Al was assembled in the middle area of coating for substrate before annealing. This fact can be interpreted due to the effect of the second step of milling, where the coating layer of Al disappeared and take place in the middle area.

Figure 8 shows the XRD patterns of the starting materials, coated substrate before and after annealing. It can be seen that the diffraction peak of Si and Al element as starting material has a dissolve or even disappear. In the MA process, those elements undergo heavy collision and become an amorphous phase due to the devastation of crystals structure (Dastanpoor et al. 2014). Hence, those elements might be undetected in XRD. This is the indication that the MA process is near complete or already complete despite the quite short MA time, i.e., 2 h. For instance, the lamellae shape is only found in the middle area of the coating layer, as shown in Figure 5a. The pulverization of the lamellae shape indicates that the MA process is almost finished, resulting in the formation of amorphous or new phases. Detail analysis of XRD in the range angle of 40-50° (Figure 9) revealed that the new phase was formed in the coating. It shows by the presence of small intensity peaks amongst the main peak of a coated substrate before annealing (Figure 9a). The peaks indicate the FeSi and Cr_5Si_3 phase. Small radii and brittle of the Si element compared with other elements is believed the reason for the formation silicide phase of Cr and Fe. The annealing treatment stimulates the formation of the new phase in the coating layer, as shown in Figure 8f and 9. Multiple phases, i.e., Cr_5Si_3, $AlCr_2$, and $AlCr_6Si$, were formed after annealing of the coated substrate. However, the existence of FeSi after annealing could not be detected, revealing the decomposition of this phase to another phase.

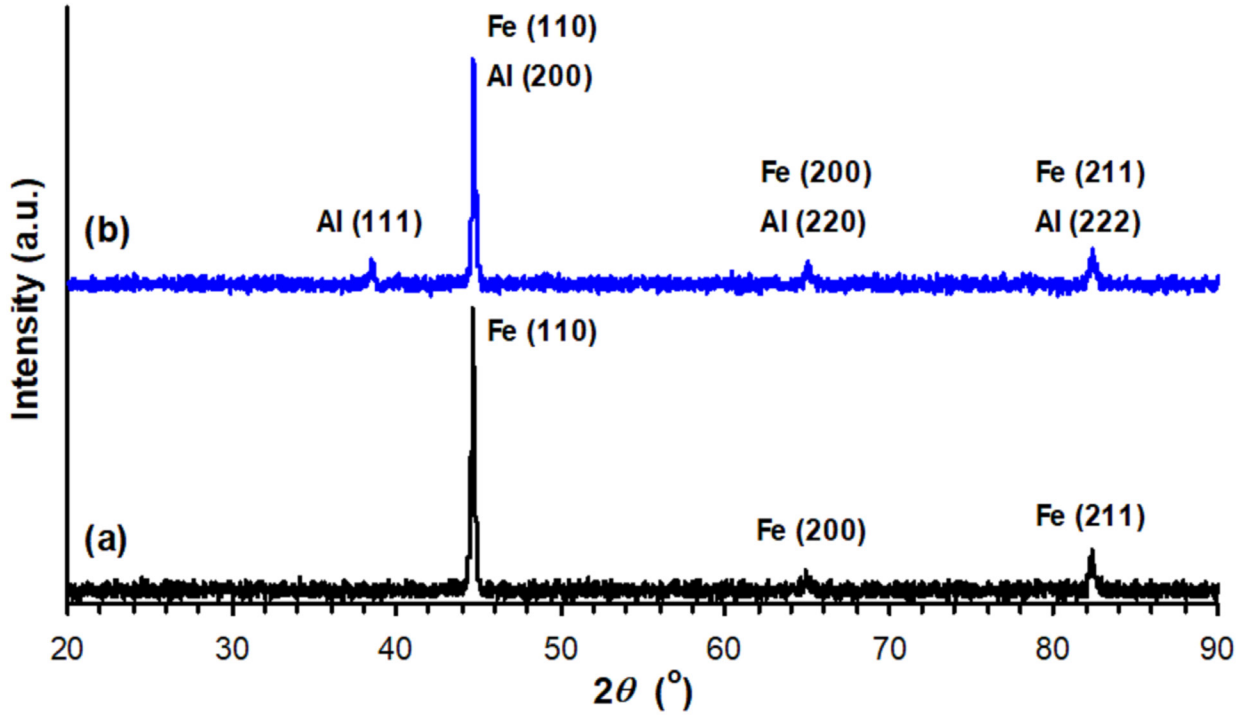

Figure 4. XRD patterns of (a) substrate and (b) first step coating of the substrate

The EDX spot analysis supported the result, which will be discussed later.

Figure 10 displays the SEM images of area 1, 2 (Figure 5a) and area 3, 4 (Figure 5b) in high magnification. Three zones are seen in Figure 10, which are light gray, dark gray and black. It indicates the difference of elemental composition in the powder, as shown in Table IV. The results reveal that the light gray zone is Cr-rich zone both in the coated substrate before and after annealing. This result was confirmed with the XRD analysis, where Cr peaks were observed before and after annealing, as shown in Figure 9. Dark gray zone in the coated substrate before annealing are Cr, Al, Fe, and Si element. The presence of other elements in the dark gray zone more likely indicated the existence of another phase, such as Cr_5Si_3, FeSi, and Fe, as observed XRD results (Figure 9). During the mixing and coating process, severe plastic deformation induced high local temperature and promoting the element diffusion between powder to powder. After annealing, the dark gray zones are converted into Si-rich. Meanwhile, the black phase in the coated substrate before and after milling is Al-rich and mix of Cr, Al, Fe, and Si, respectively. Generally, the EDX analysis cannot identify all of the phases in XRD analysis. It may be caused that the formation of intermetallic compound randomly distribution in coating with small size.

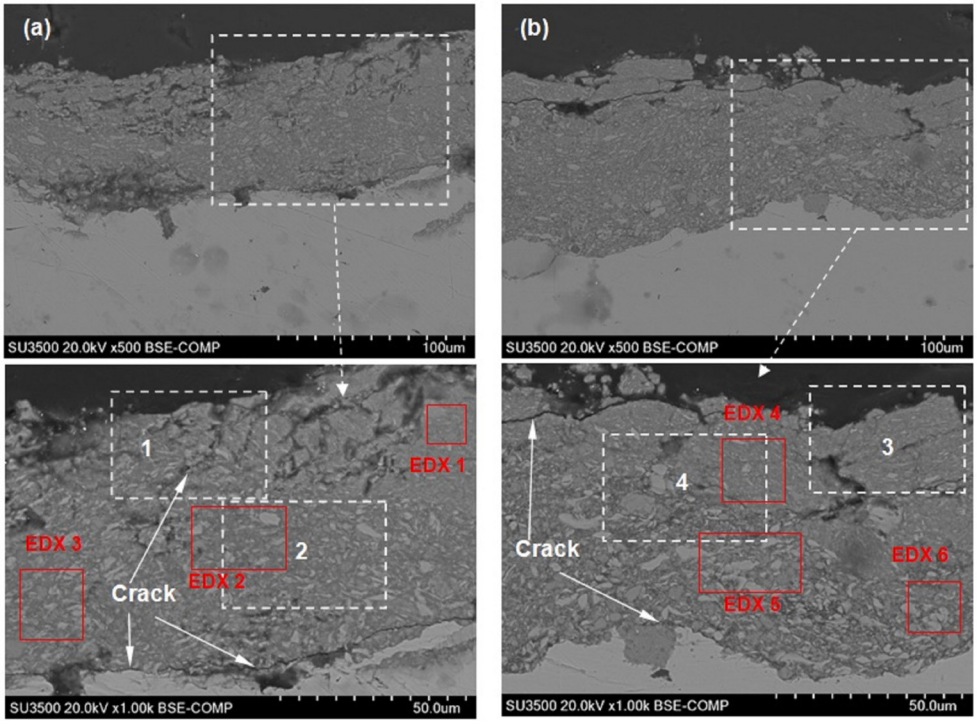

Figure 5. Cross-section SEM images of coated substrate (a) before and (b) after annealing at 650 °C.

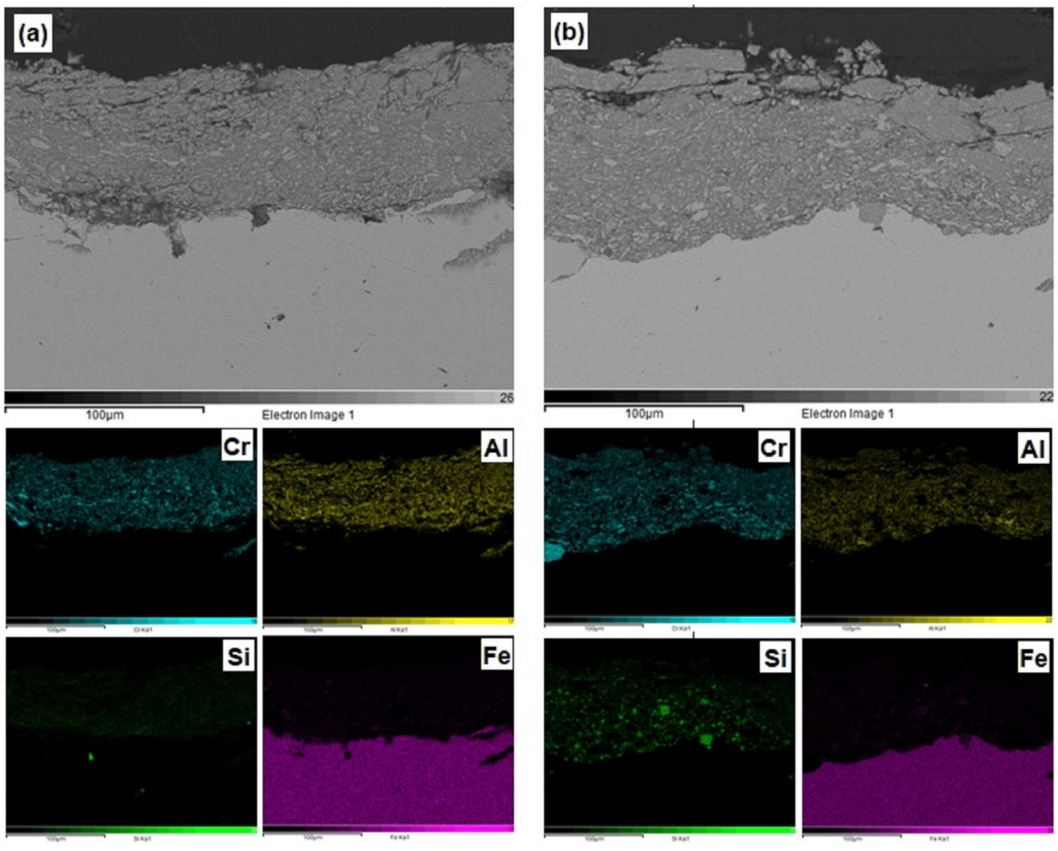

Figure 6. EDX elemental mapping of coated substrate (a) before and (b) after annealing at 650 °C.

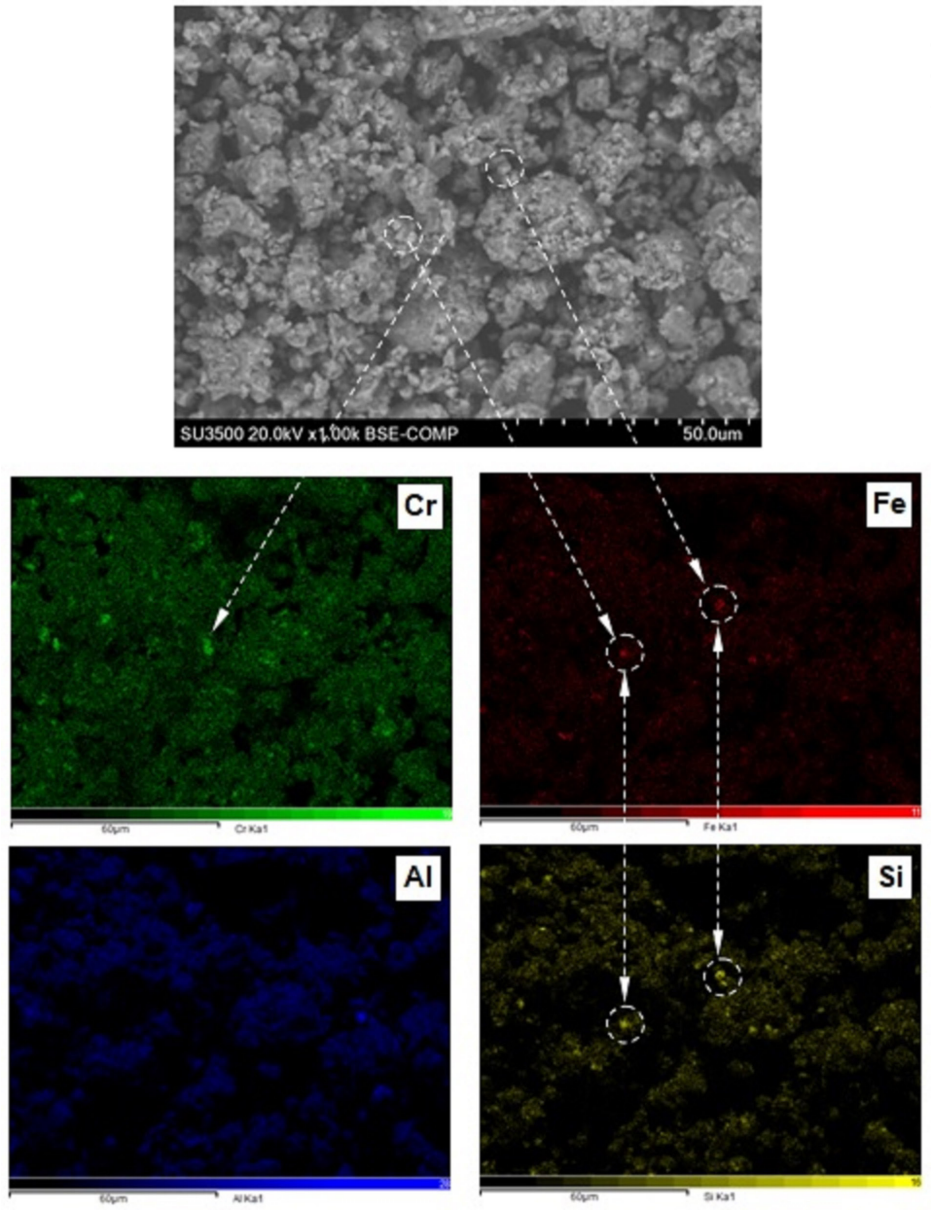

Figure 7. SEM images and elemental distribution of CrAlFeSi powder after deposition process.

Table III. EDX analysis of the coated substrate for the position 1-6 marked in Figure 3a and Figure 3b.

Position	Element (atomic%)			
	Cr	Al	Fe	Si
EDX 1	30.68	36.98	12.71	19.63
EDX 2	26.03	40.67	12.35	20.95
EDX 3	31.77	36.66	10.64	20.93
EDX 4	31.30	37.38	11.06	19.96
EDX 5	34.97	32.93	10.82	21.28
EDX 6	35.48	34.02	10.18	20.31

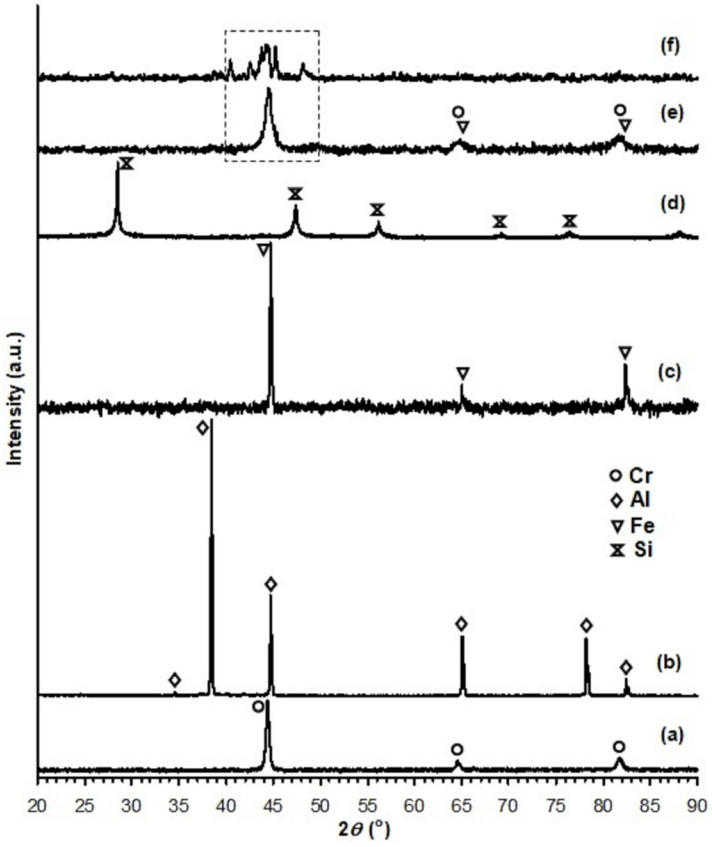

Figure 8. XRD pattern of (a) Cr, (b) Al, (c) Fe, (d) Si, coated substrate (e) before and (f) after annealing at 650 °C.

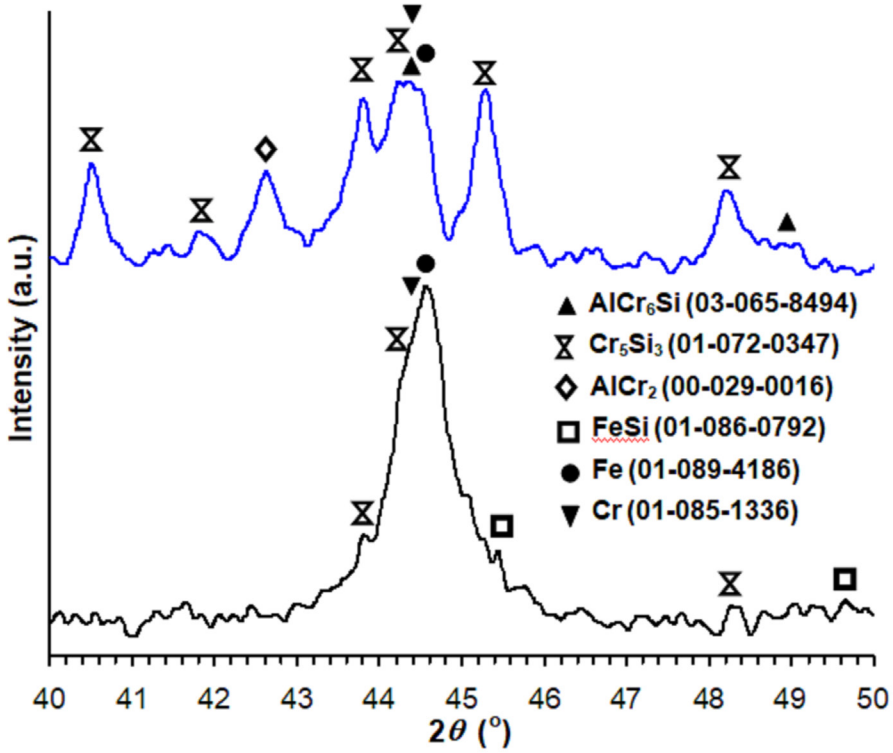

Figure 9. XRD pattern details of coated substrate without and with annealing in Figure 7e and Figure 7f, respectively

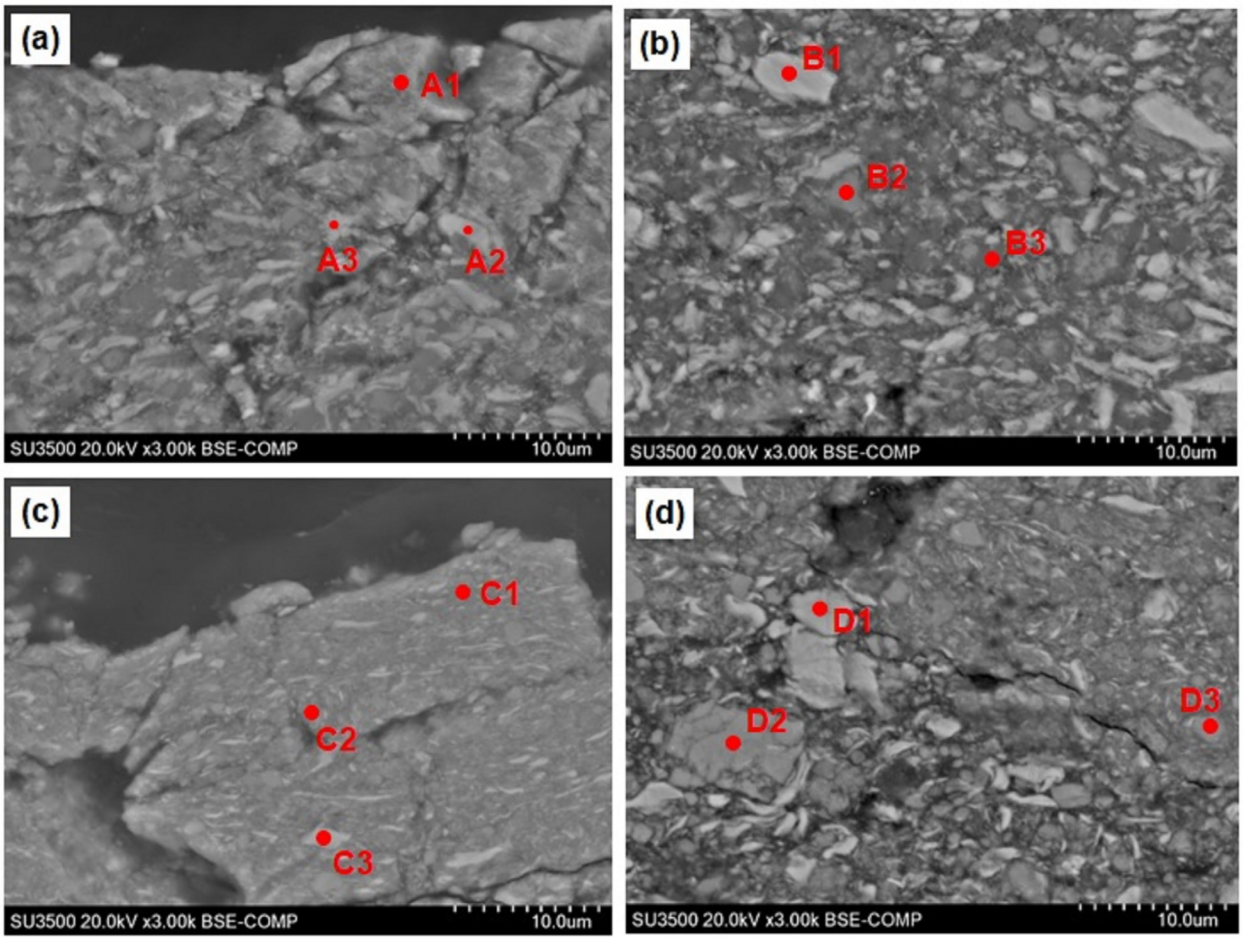

Figure 10. Localized magnification of marked position 1 (a), 2 (b), 3 (c) and 4 (d) in Figure 3.

Table IV. EDX point analysis of Figure 5.

Marked	Element (at.%)				Remark
	Al	Si	Cr	Fe	
A1	42.50	19.03	26.75	11.72	Dark Gray
A2	6.97	3.36	88.24	1.43	Light gray
A3	17.98	19.94	57.80	4.28	Light gray
B1	-	0.54	98.77	0.69	Light gray
B2	35.80	27.90	10.16	26.14	Dark gray
B3	52.52	14.58	16.45	16.45	Black
C1	19.92	40.41	20.04	19.64	Dark gray
C2	45.29	13.41	33.88	7.42	Dark gray
C3	4.79	6.54	86.09	2.59	Light gray
D1	4.61	0.66	93.01	4.61	Light gray
D2	-	60.45	3.95	35.60	Dark gray
D3	16.23	45.76	13.33	24.69	Dark gray

The oxidation resistance of the coated substrate

Figure 11 presents the oxidation kinetics of the uncoated and coated substrate before and after annealing for 20h-cycles. Indeed, the substrate without coating showed a very high mass gain compared to the coated substrate, as shown in Figure 11. The mass gain increases by a factor of 10 after 8 cycles for the uncoated substrate, indicating the effectiveness of the coating layer to prevent oxidation. The weight gain of the uncoated and coated substrate in the first cycle of oxidation was > 30 mg/cm^2 and < 2 mg/cm^2, respectively. The high oxidation resistance of the coated substrate might be attributed to the formation of new phases, which prevent severe oxidation in the substrate. Interestingly, the mass gain for the coated substrate before and after annealing did not differ significantly, as can be seen in the inset of Figure 11. However, detailed observation shows that the mass gain of the coated substrate increases as a linear function of the number of oxidation cycles. It more likely due to the formation of the severe stress cracks of scale on the surface. As soon as a crack appeared, the substrate would directly contact air, accelerating the oxidation rate and forming a new oxide scale (Cheng et al. 2016). Besides that, the spallation of the protective oxide scale also intensifies the oxidation process occurring during the cyclic oxidation (Aryanto et al. 2020). Moreover, it also might happen due to long oxidation time, which decreased the protection of the substrate by the oxide layer.

In order to have a clear understanding of the oxidation behavior of the coated substrate before and after annealing, the generated phases during oxidation were examined from the XRD patterns in Figure 12. The result shows that there is the formation of intermetallic $AlCr_6Si$, $AlCr_2Fe_2O_3$, and Al_2O_3 in the coated substrate after oxidation, both for before (Figure 12a) and after annealing (Figure 12b). The presence of Fe_2O_3 phase in the coated substrate might be from the nodule, which was existed in both substrates, as shown in Figures 13 and 14. The detail discussion

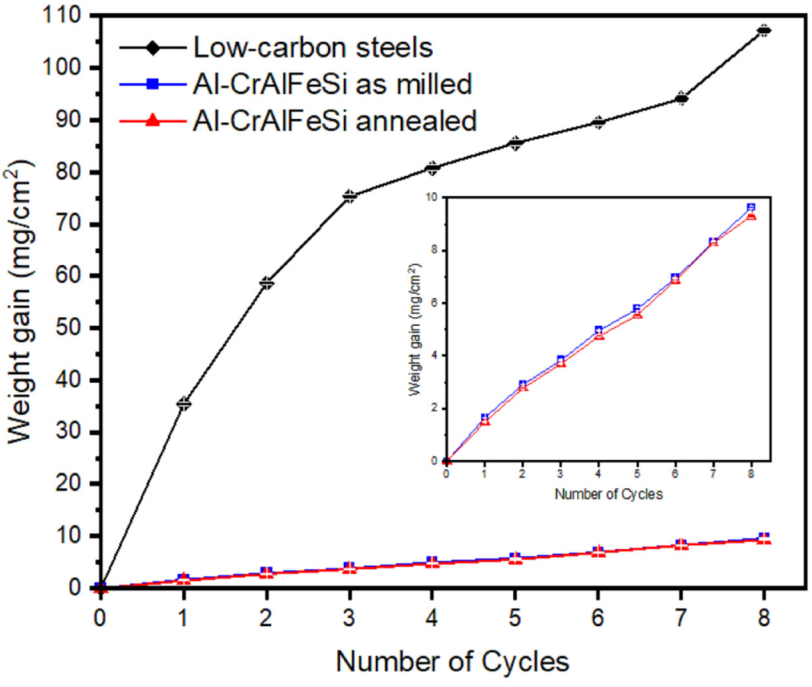

Figure 11. The cyclic oxidation curves of uncoated and coated substrate after oxidation at 800 °C for 20 h in one cyclic.

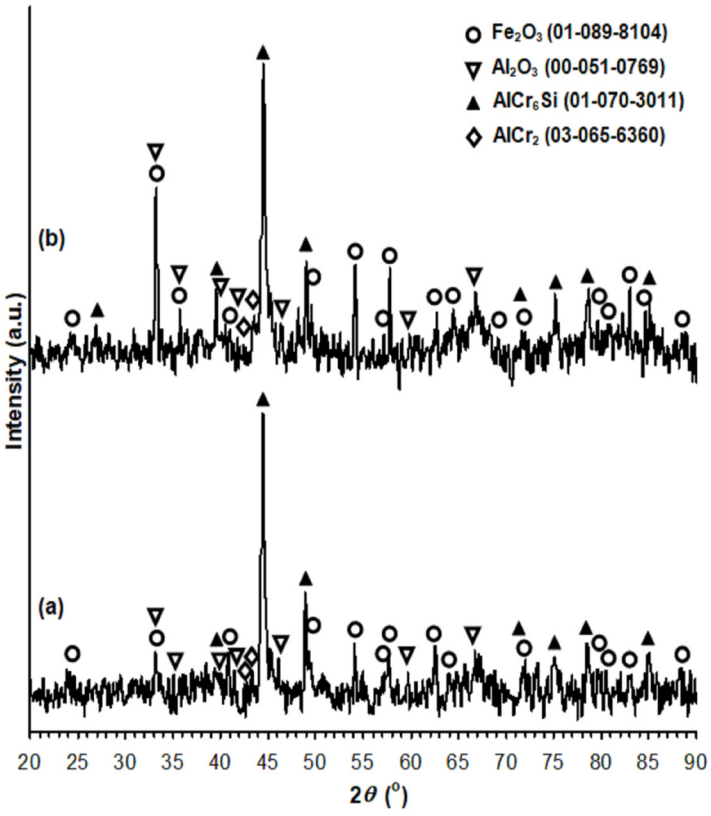

Figure 12. XRD patterns of coated substrate after cyclic oxidation for 8 cycles at 800 °C.

about the nodule was reported in our previous work (Sudiro et al. 2018).

Figure 13 and Figure 14 show the cross-section images of the coated substrate before and after annealing, respectively, after oxidation at 800 °C for 8 cycles. Although the oxidation was performed at high temperature, the presence of microcrack is spotted in the coated substrate before annealing (Figure 13). This phenomenon showed that the diffusion did not occur and led to the formation of a microcrack. On the other hand, the presence of microcrack is not seen in the coated substrate after annealing. It can be concluded that the annealing treatment at 650 °C improves the bonding between the coating layer and the substrate interface (Figure 5b). The existence of microcracks, both in the coated substrate before and after annealing, might be attributed to the increase of internal stress as an effect of repetitive heating and cooling during cyclic oxidation. One notable finding in this study is the presence of the oxide scale both in the coated substrate before (Figure 13) and after annealing (Figure 14). The thickness of the oxide scale is 1.25 - 1.80 µm. The observation of the coating-oxide interface shows that the oxide scale has good bonding with no crack or porous. According to EDX mapping of the coated substrate before (Figure 15a) and after annealing (Figure 15b), the oxide scale is composed of Al and O. In addition, EDX point analysis of the oxide scale confirmed that the major elements are Al and O, as shown in Figure 16 and Table V. For instance, the amount of Al and O in the oxide scale coated substrate before annealing (30.92 and 66.61 at %, respectively) corresponds to the composition of Al_2O_3. The Al_2O_3 scale is formed due to the reaction between Al (outward diffusion) and O (inward diffusion) from the air. The Al_2O_3 layer on the surface blocks oxygen

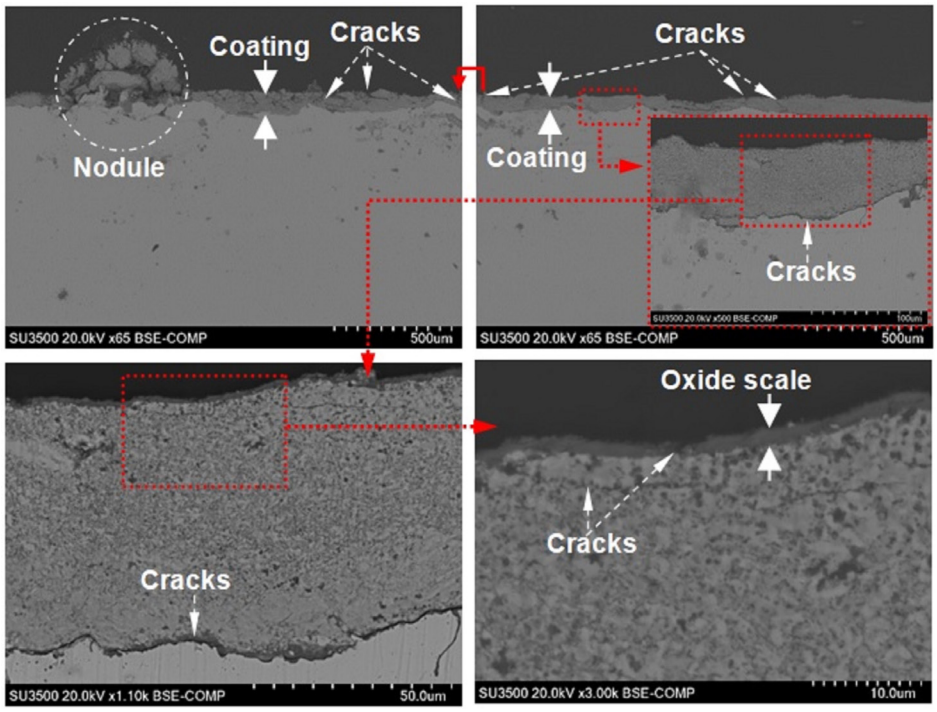

Figure 13. Cross-section morphologies of the coated substrate without annealing after oxidation at 800 °C for 8 cycles.

diffusion into the substrates, thus improves the oxidation resistance of the coated substrate.

The formation of Al_2O_3 in the surface diffusion zone can also be explained by classical thermodynamic theory. The Gibbs free energies ($\Delta G°$) of Al_2O_3, SiO_2, Cr_2O_3, and Fe_2O_3 at 800 °C are -891.144, -717.537, -568.661, and -360.775 kJ, respectively. This calculation reveals that Al_2O_3 has the lowest Gibbs free energy, which means the formation of Al_2O_3 is more favorable compare to SiO_2, Cr_2O_3, and Fe_2O_3.

Figure 16 shows EDX point analysis of the coating layer after oxidation for coated substrate before and after annealing. The quantitative analysis of the EDX result is shown in Table V. Interestingly, the amount of O is higher near the surface compared to the middle area, as shown in Table V. For instance, in the sample without annealing (Figure 16a), the amount of O in point 4 is higher than point 7, while in sample with annealing (Figure 16b), the amount of O in point 7 is higher than point 4. This phenomenon is likely due to the inward diffusion of oxygen into the coating layer during oxidation. In addition, two phases are discovered in the coating layer, i.e., black and dark gray phases. The black phases belong to a region with microholes in the coating before oxidation (Chen et al. 2016), while the dark gray phases are the dense phases without microholes.

Table VI shows the net weight gain of the coated substrate after oxidation by different coating methods. It can be seen that the oxidation resistance of the coated substrate depends on the deposited element/compound on the substrate. Indeed, the deposition of ceramic (Nguyen et al. 2018) or intermetallic (Erfanmanesh & Bakhshi 2018) reduces the weight gain significantly. However, the deposition of this compound leads to minimum diffusion into the substrate (Nguyen et al. 2018). In this study, the weight gain of the coated substrate is lower compared to other methods, for instance, electroplating, thermal spray, and one step MA indicating that two steps coating by MA is an alternative method to minimize oxidation in the low carbon steel.

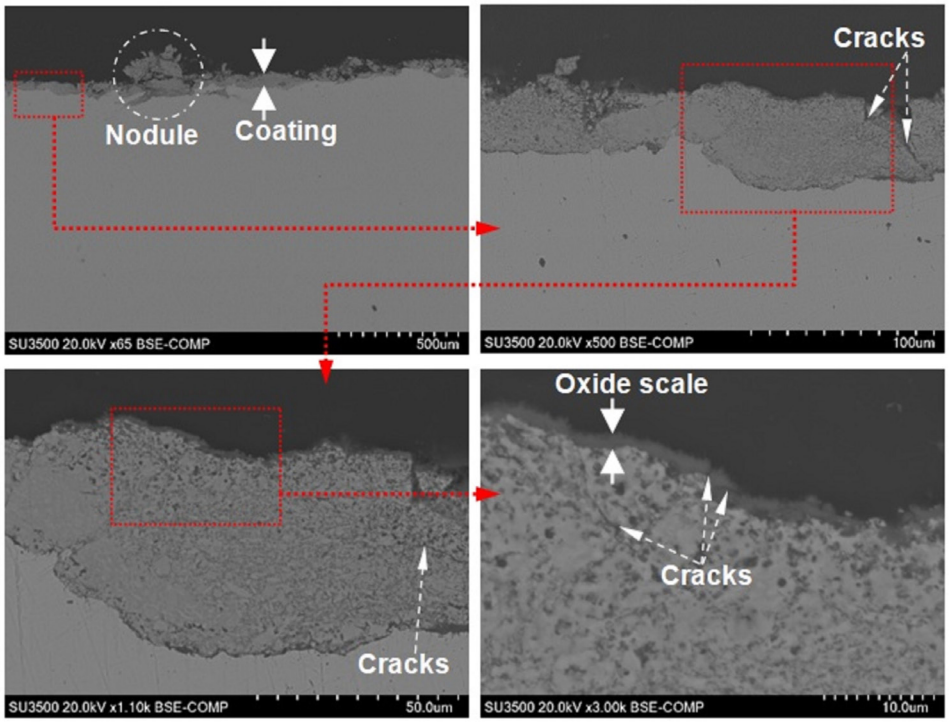

Figure 14. Cross-section morphologies of the coated substrate with annealing after oxidation at 800 °C for 8 cycles.

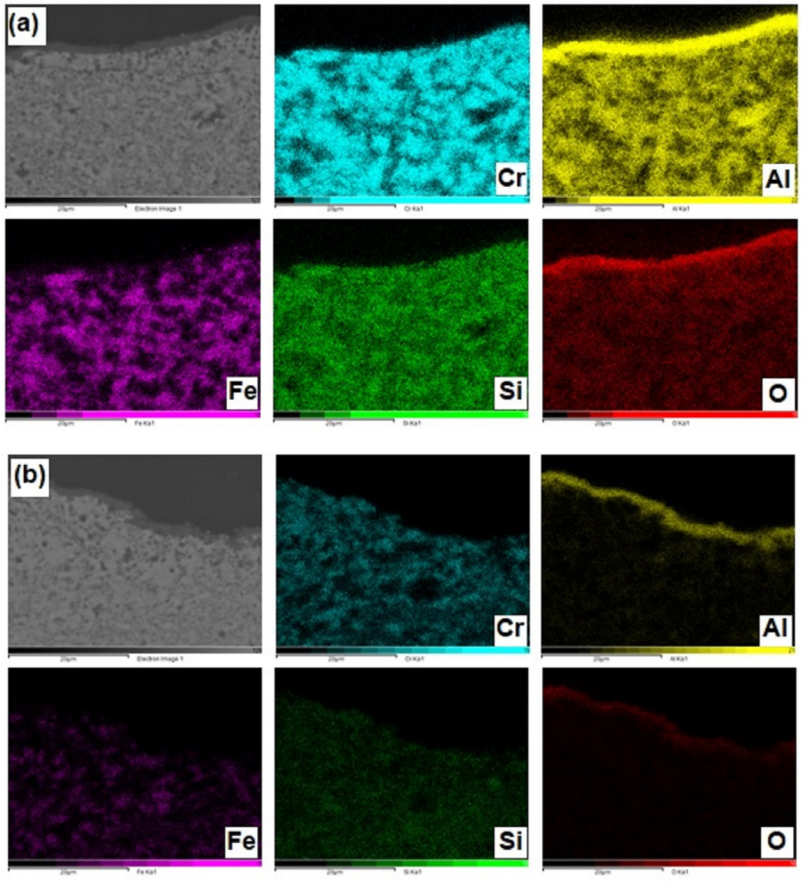

Figure 15. Cross-section SEM images and element mapping of coated substrate after oxidation for the coated substrate (a) before and (b) after annealing.

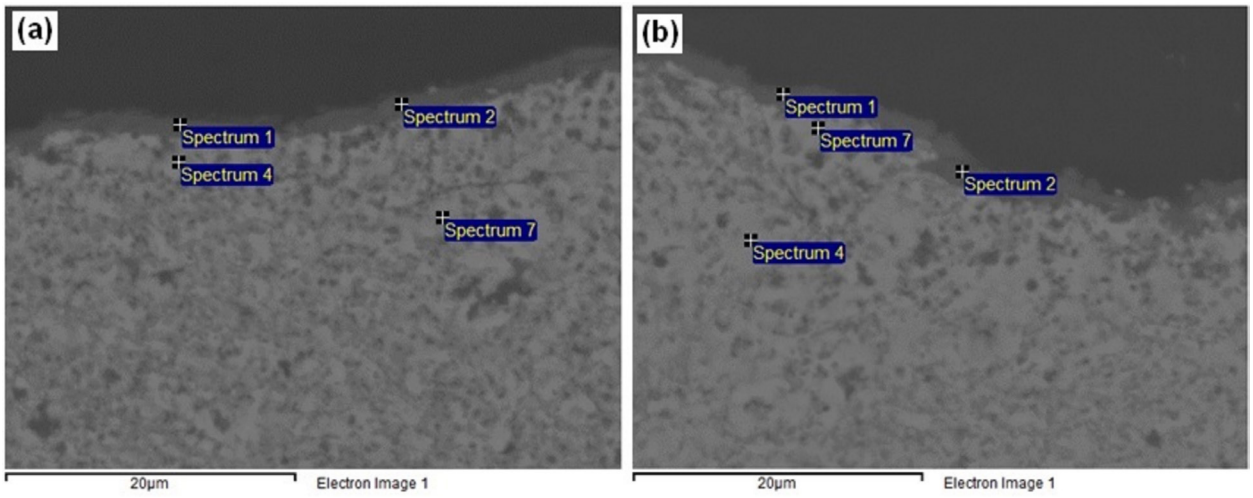

Figure 16. EDX point analysis of the coated substrate after oxidation for the coated substrate (a) before and (b) after annealing.

Table V. EDX point analysis of Figure 11.

Position	CrAlFeSi coating as milled						CrAlFeSi coating annealed				
	Element (at.%)						Element (at.%)				
	O	Al	Si	Cr	Fe		O	Al	Si	Cr	Fe
Spectrum 1	66.61	30.92	0.81	1.21	0.45		65.99	32.37	0.72	0.71	0.21
Spectrum 2	65.27	32.39	0.82	1.16	0.36		63.75	33.66	0.86	1.45	0.27
Spectrum 4	23.52	29.37	12.71	13.88	20.52		12.95	20.18	16.56	26.02	24.30
Spectrum 7	16.39	29.84	14.07	11.90	27.79		22.07	15.57	18.07	33.79	10.50

Table VI. Previous research results on the weight gain of the substrate after oxidation.

Coating-method	Coating elements	Coating Thickness (µm)	Oxidation methods	Oxidation temperature (°C)	Times	Weight gain (mg/cm^2)
Electroplating (Farrokhzad, 2017)	Ni-P-BN(h)	29 – 50	Isothermal	700	96 h	20
Thermal spray (Premkumar and Balasubramanian, 2019)	Cr-Ni-C	280 – 320	Cyclic oxidation	900	50 cyclic	2.15 – 65.98
Slurry spray (Nguyen et al. 2018)	Glass Ceramics	162	Isothermal	800	540 min	4.33
Mechanical alloying (Sudiro et al. 2018)	Cr-Al	80 – 120	Cyclic oxidation	800	160 h	10.5 – 23.3
This study	Cr-Al-Fe-Si	75	Cyclic oxidation	800	160 h	9.5

CONCLUSIONS

Two steps coating prepared by the mechanical alloying method has been performed successfully. The first step was done to deposit Al powder on the substrate by mechanical alloying method for 1 h. Smooth coating of Al can be observed without the presence of holes and cracks. This first step bridges the second step since Al has been known as an excellent binding agent. The second step coating was aimed to deposit the main composition, i.e., CrAlFeSi powder, using mechanical alloying for 2 h. The coated substrate was annealed, and its oxidation properties were compared to the coated substrate without annealing. The microstructure of the as-annealed coated substrate was considerably improved compared to the coated substrate before annealing. It is concluded that the microholes and microcrack can be minimized by annealing the coated substrate. Despite the short processing time (2 h MA), the multiple intermetallic phase, i.e., Cr_5Si_3, $AlCr_2$, and $AlCr_6Si$, can be observed in the coated substrate after annealing. It should be noted that the oxidation resistance of the coated substrate is enhanced significantly by two steps coating. The weight gain of the coated substrate after the cyclic oxidation test can be suppressed by the factor of 10, after introducing CrAlFeSi layer by two steps coating. The enhanced oxidation properties of the coated substrate might also be attributed to the formation of Al_2O_3 scale on the coating layer. The coated substrate before and after annealing possesses relatively similar oxidation properties. However, the annealing of the coated substrate presents a better microstructure compared to the coated substrate without annealing

Acknowledgments

This research was supported by Ministry of Research, Technology and Higher Education, Indonesia under Grant No. 013/P/RPL-LIPI/INSINAS-2/VII/2018 and LPDP Grant No. 31/F1/PKS-KCOVID-19.B/VI/2020. The authors are grateful to the Research Center for Physics - LIPI for providing the research facilities. The authors also acknowledge Mrs. Retno Kusumaningrum, M.Sc. for analyzing the microstructure using image processing software.

REFERENCES

ARYANTO D, NOVIYANTO A, SUDIRO T, SUKARTO A, BAMBANG W, SEBAYANG P & ROCHMAN NT. 2020. Effect of annealing temperature on the oxidation behavior of ferrosilicon-aluminum-coated low carbon steel by mechanical alloying. J Alloys Compd 821: 153493.

ARYANTO D & SUDIRO T. 2018. Preparation of ferrosilicon-aluminium coating using a mechanical alloying technique: Study of thermal annealing on their structural characteristics. Surf Coatings Technol 337: 35-43.

BAFANDEH MR, OMIDI A & IRANKHAH A. 2017. In situ coating of low carbon steel with Ni-Al-Fe powder mixture via mechanical alloying. Surf Coatings Technol 315: 268-273.

CANAKCI A, ERDEMIR F, VAROL T & OZKAYA S. 2013. Formation of Fe-Al intermetallic coating on low-carbon steel by a novel mechanical alloying technique. Powder Technol 247: 24-29.

CHEN C, ZHANG J, DUAN C, FENG X & SHEN Y. 2016. Investigation of Cr-Al composite coatings fabricated on pure Ti substrate via mechanical alloying method: Effects of Cr-Al ratio and milling time on coating, and oxidation behavior of coating. J Alloys Compd 660: 208-219.

CHENG X, FAN L, LIU L, DU K & WANG D. 2016. Effect of doping aluminum and yttrium on high-temperature oxidation behavior of Ni-11Fe-10Cu alloy. JRare Earths 34: 1139-1147.

DASTANPOOR E, ENAYATI MH & KARIMZADEH F. 2014. Synthesis of Cu-Zr-Al/Al_2O_3 amorphous nanocomposite by mechanical alloying. Adv Powder Technol 25: 519-523.

ERFANMANESH M & BAKHSHI SR. 2018. Oxidation behavior of nanostructured and conventional $MoSi_2$ plasma-sprayed coatings. Ceram Int 44: 15839-15844.

FARROKHZAD MA. 2017. High temperature oxidation behaviour of autocatalytic Ni-P-BN(h) coatings. Surf Coatings Technol 309: 390-400.

LASZCZYŃSKA A, WINIARSKI J, SZCZYGIEŁ B & SZCZYGIEŁ I. 2016. Electrodeposition and characterization of Ni-Mo-ZrO_2composite coatings. Appl Surf Sci 369: 224-231.

LI B, DING R, SHEN Y, HU Y & GUO Y. 2012. Preparation of Ti-Cr and Ti-Cu flame-retardant coatings on Ti-6Al-4V using a high-energy mechanical alloying method: A preliminary research. Mater Des 35: 25-36.

LI Y, CHEN C, DENG R, FENG X & SHEN Y. 2014. Microstructure evolution of Cr coatings on Cu substrates prepared by mechanical alloying method. Powder Technol 268: 165-172.

MOHAMMADNEZHAD M, SHAMANIAN M & ENAYATI MH. 2012. Formation of nanostructured NiAl coating on carbon steel by mechanical alloying. Appl Surf Sci 263: 730-736.

MOHAMMADNEZHAD M, SHAMANIAN M, ENAYATI MH & SALEHI M. 2013. Influence of annealing temperature on the structure and properties of the nanograined NiAl intermetallic coatings produced by using mechanical alloying. Surf Coatings Technol 217: 64-69.

NGUYEN MD, BANG JW, KIM YH, BIN AS, HWANG KH, PHAM VH & KWON WT. 2018. Slurry spray coating of carbon steel for use in oxidizing and humid environments. Ceram Int 44: 8306-8313.

PREMKUMAR K & BALASUBRAMANIAN KR. 2019. Evaluation of cyclic oxidation behavior and mechanical properties of nanocrystalline composite HVOF coatings on SA 210 grade C material. Eng Fail Anal 97: 635-644.

ROMANKOV S, HAYASAKA Y, KALIKOVA G, KOMAROV SV, HAYASHI N & KASAI E. 2009a. TEM study of TiN coatings fabricated by mechanical milling using vibration technique. Surf Coatings Technol203: 1879-1884.

ROMANKOV S, KOMAROV SV, VDOVICHENKO E, HAYASAKA Y, HAYASHI N, KALOSHKIN SD & KASAI E. 2009b. Fabrication of TiN coatings using mechanical milling techniques. Int J Refract Met Hard Mater 27: 492-497.

ROMANKOV S, SHA W, KALOSHKIN SD & KAEVITSER K. 2006. Fabrication of Ti-Al coatings by mechanical alloying method. Surf Coatings Technol 201: 3235-3245.

SABA F, KABIRI E, KHAKI JV & SABZEVAR MH. 2016. Fabrication of nanocrystalline TiC coating on AISI D2 steel substrate via high-energy mechanical alloying of Ti and C. Powder Technol 288: 76-86.

SUDIRO T, HIA AIJ, CISWANDI, ARYANTO D, HERMANTO B, WISMOGROHO AS & SEBAYANG P. 2018. High temperature cyclic oxidation resistance of 50Cr-50Al coatings mechanically alloyed on low carbon steel. J Alloys Compd 732: 655-665.

SZYMAŃSKI K, HERNAS A, MOSKAL G & MYALSKA H. 2015. Thermally sprayed coatings resistant to erosion and corrosion for power plant boilers - A review. Surf Coatings Technol 268: 153-164.

WISMOGROHO AS, IRAWANTO H, WIDAYATNO WB, NOVIYANTO A, SURYADI ROCHMAN NT & SUEYOSHI H. 2009. Iron Aluminide Coating of Structural Steel by Mechanical Alloying Followed by Annealing. J Japan Soc Powder Metall 56: 427-432.

YANG GJ, WANG HT, LI CJ & LI CX. 2011. Effect of annealing on the microstructure and erosion performance of cold-sprayed FeAl intermetallic coatings. Surf Coatings Technol 205: 5502-5509.

ZADOROZHNYY VY, SHAHZAD A, PAVLOV MD, KOZAK DS, CHIRKOV AM, ZAGREBIN DS, KHASENOVA RS, KOMAROV SV & KALOSHKIN SD. 2017. Synthesis of the Ni-Al coatings on different metallic substrates by mechanical alloying and subsequent laser treatment. J Alloys Compd 707: 351-357.

ZHAN Z, HE Y, WANG D & GAO W. 2006. Low-temperature processing of Fe-Al intermetallic coatings assisted by ball milling. Intermetallics 14: 75-81.

How to cite

ARYANTO D, NOVIYANTO A, SUNDAWA RY, SUDIRO T, WISMOGROHO AS, WIDAYATNO WB & SEBAYANG P. 2020. Two steps CrAlFeSi coating on low carbon steel prepared by mechanical alloying and its oxidation properties. An Acad Bras Cienc 92: e20200524. DOI 10.1590/0001-3765202020200524.

Manuscript received on April 11, 2020;
accepted for publication on July 13, 2020

DIDIK ARYANTO[1]
https://orcid.org/0000-0001-5123-8551

ALFIAN NOVIYANTO[2,3]
https://orcid.org/0000-0002-6371-6765

RISMA Y. SUNDAWA[1]
https://orcid.org/0000-0003-1849-3459

TOTO SUDIRO[1]
https://orcid.org/0000-0001-7872-914X

AGUS S. WISMOGROHO[1]
https://orcid.org/0000-0002-7628-2310

WAHYU B. WIDAYATNO[1]
https://orcid.org/0000-0003-1570-8100

PERDAMEAN SEBAYANG[1]
https://orcid.org/0000-0002-8590-0678

[1]Research Center for Physics, Indonesian Institute of Sciences, PUSPIPTEK, South Tangerang, 15314, Banten, Indonesia

[2]Nano Center Indonesia, Jl. PUSPIPTEK, South Tangerang, 15314, Banten, Indonesia

[3]Department of Mechanical Engineering, Mercu Buana University, Jl. Meruya Selatan, Kebun Jeruk, 11650, Jakarta, Indonesia

Correspondence to: **Didik Aryanto**
E-mail: didi027@lipi.go.id

Author contributions

DA conceived and designed the research, performed the analysis, collect the data, wrote the first draft of manuscript. AN conceived and designed the research, performed the analysis, revised the manuscript, contributed equally as the first author. RYS, TS, ASW, WBW, PS performed the analysis, discussed the results, read and approved the final manuscript.